Letter

Evolution of room-temperature magnon gas: Toward a coherent Bose-Einstein condensate

Timo B. Noack [1,*] Vitaliy I. Vasyuchka [1,†] Anna Pomyalov [2]
Victor S. L'vov,[2] Alexander A. Serga [1] and Burkard Hillebrands [1]

[1]*Fachbereich Physik and Landesforschungszentrum OPTIMAS, Technische Universität Kaiserslautern, 67663 Kaiserslautern, Germany*
[2]*Department of Chemical and Biological Physics, Weizmann Institute of Science, Rehovot 76100, Israel*

(Received 22 January 2021; revised 24 August 2021; accepted 25 August 2021; published 16 September 2021)

The appearance of spontaneous coherence is a fundamental feature of a Bose-Einstein condensate and an essential requirement for possible applications of the condensates for data processing and quantum computing. In the case of a magnon condensate in a magnetic crystal, such computing can be performed even at room temperature. We study the process of the formation of a coherent magnon condensate by direct detection of microwave radiation emitted by magnons in a parametrically driven yttrium iron garnet bulk sample of a special shape. We show that after switching off the parametric pumping, the overpopulated magnon gas evolves to a state, whose coherence is only limited by the natural magnon relaxation into the crystal lattice.

DOI: 10.1103/PhysRevB.104.L100410

The Bose-Einstein condensate (BEC) is a state of matter encompassing a macroscopically large number of bosons that occupy the lowest quantum state, demonstrating coherence at macroscopic scales [1–5]. This phenomenon was observed and investigated in atomic systems such as ^{4}He, ^{3}He (where the role of bosons is played by Cooper pairs of fermionic ^{3}He atoms), and in ultracold trapped atoms [6,7]. BECs were also found in systems of bosonic quasiparticles such as polaritons [8] and excitons [9] in semiconductors, photons in microcavities [10], as well as magnons in superfluid ^{3}He [11] and magnetic crystals [12–14].

The presence of macroscopic coherence is of fundamental importance for understanding the physical properties of BECs, including exciting phenomena such as superconductivity and superfluidity. Furthermore, there is a range of novel effects and applications that exploit the coherence of macroscopic BEC wave functions [15–20], especially in the rapidly developing field of quantum computing [17–20]. Unlike already demonstrated superconductor-based quantum computers, which operate at temperatures around 20 μK [21], BEC-based qubits can be implemented at significantly higher temperatures. For instance, in ferrimagnetic yttrium iron garnet ($Y_3Fe_5O_{12}$, YIG) crystals [22], a magnon BEC [12] and supercurrents [23] are formed even at room temperature.

The magnon condensate is usually created in YIG by the parametric pumping of magnons in an external microwave electromagnetic field. In this process [24,25], external microwave photons of frequency ω_p and wave number $q_p \simeq 0$ split into two magnons with the frequency $\omega_m = \omega_p/2$ and wave vectors $\pm\mathbf{q}_m$. They populate a gaseous magnon distribution with internal interactions provided by the four-magnon scattering processes $2 \Leftrightarrow 2$. Eventually, the magnon gas thermalizes to the bottom of the frequency spectrum [26,27] and if the applied pumping power exceeds a certain threshold, a BEC forms there [12]. In in-plane magnetized YIG films, magnons condense at two equivalent frequency minima $\omega_{min}(\pm\mathbf{q}_{BEC})$.

The magnon BEC is conveniently studied by means of Brillouin light scattering (BLS) spectroscopy [12,13], delivering information about the magnon spectral density distribution. Unfortunately, due to the limited frequency resolution of the optical Fabry-Pérot interferometers used in BLS facilities, the coherence of a magnon BEC cannot be proven directly. Due to the phase insensitivity of the BLS process, studies of the BEC relaxation dynamics employing time-resolved BLS spectroscopy fail to account for BEC dephasing. The insufficient frequency resolution makes it impossible to separate the relaxation dynamics of condensed and thermal magnons. Moreover, the possible outflow of the condensate from a spatially localized probing light spot complicates the interpretation of the obtained experimental results (see Ref. [28] and the corresponding discussion in Ref. [29]).

Alternatively, magnon BEC coherence can be tested indirectly by the observation of phenomena such as quantized vorticity [30], supercurrents [23], Bogoliubov waves [31], or Josephson oscillations [32], which are canonical features of both atomic and quasiparticle quantum BECs. Our studies of some of these phenomena [23,31–34] have shown that they occur only in a freely evolving magnon gas after pumping is turned off. This takes place probably because the intense pumping process prevents condensation by heating the magnon gas [13] and mixing the magnon frequencies near the bottom of their spectra [29]. The observation of these effects indicates the presence of a time-dependent BEC coherence, but leaves open the question about the degree of coherence.

Previous studies for the qualitative characterization of BEC coherence were made using a novel high-resolution magneto-optical Kerr-effect spectroscopy technique [35,36], microwave spectroscopy of electromagnetic signals emitted at the ferromagnetic resonance frequency due to the confluence of bottom magnons with opposite wave vectors [37,38], and by BLS observations of the interference of $\pm\mathbf{q}_{BEC}$ magnon condensates [30]. They demonstrate a low modulation depth

*tnoack@rhrk.uni-kl.de
†vasyuchka@physik.uni-kl.de

of the interference patterns [30], a rather broad frequency spectral BEC line [37], and an increase in the BEC linewidth when the pumping power exceeds the threshold of BEC formation [36]. These results themselves are certainly interesting and important. However, without additional data on the temporal evolution of coherence, their interpretation is difficult. In addition, in many previous works, both the pumping of magnons and the observation and analysis of the BEC state were performed during the pumping action. Although this approach is, generally speaking, acceptable, one cannot rule out perturbation of the BEC state by the pumping field. In the scenario demonstrated here, the critical magnon density required for the BEC formation is achieved by the application of strong pumping pulses, which clearly perturb the BEC state and, as a consequence, lead to a strong broadening of its linewidth during pumping. In this case, the BEC is formed after the pump pulse is turned off at the time of its unperturbed decay.

The main goal of this Letter is to understand the time evolution of the magnon gas toward a coherent BEC state. By the direct measurement of microwave radiation from a bulk YIG sample, we show that the frequency-broadband emission spectrum, detected during the pumping action, transforms after the end of pumping into a sharp spectral peak at the lowest frequency of the magnon spectrum. This peak is formed earlier and gets pronounced with increasing pumping power and, consequently, with the density of parametrically pumped magnons. This spontaneously arising state becomes Lorentz shaped, and its width is consistent with the magnetic relaxation frequency into the YIG crystal lattice. The appearance of this peak is associated with the formation of the magnon BEC, whose coherence is, therefore, limited only by the natural magnon decay.

The low-temperature magnon BEC and related effects in helium were discovered and investigated employing the inductive detection technique [11,39–45]. Also, a similar technique was utilized in recent studies of induction signals in perpendicularly magnetized YIG films [46]. This is possible because, in these cases, a homogeneous precession of the magnetization is registered, which is strongly coupled with the high-frequency electromagnetic field and, therefore, can be easily detected by inductive antennas. In in-plane magnetized YIG films used in the previous room-temperature BEC studies, the condensed magnons have a wavelength of about a few micrometers and are thus weakly coupled to the electromagnetic field, making them difficult to detect via directly emitted radiation. The main idea of our experiment is to use a YIG cuboid bulk sample to enhance this coupling. The experimental setup is shown in Fig. 1(a). The YIG sample sized $0.3 \times 0.3 \times 0.6$ mm^3 is magnetized along its long side, which is oriented along the x coordinate axis. Due to the demagnetization effect, the static magnetic field $H(x)$ inside such a sample [blue line in Fig. 1(b)] is smaller at its edges than in the middle. For a slowly spatially varying magnetic field $H(x)$, the magnon frequency may be considered as an adiabatic invariant: $\omega[\mathbf{q}(x), H(x)] = \text{const}$, while the wave vector becomes position dependent $\mathbf{q} \to \mathbf{q}(x)$ [47,48].

For the BEC magnons, this frequency is equal to the frequency of the spectrum minimum $\omega_{\min}$ in the central part of the sample [marked by point A in Fig. 1(b)]:

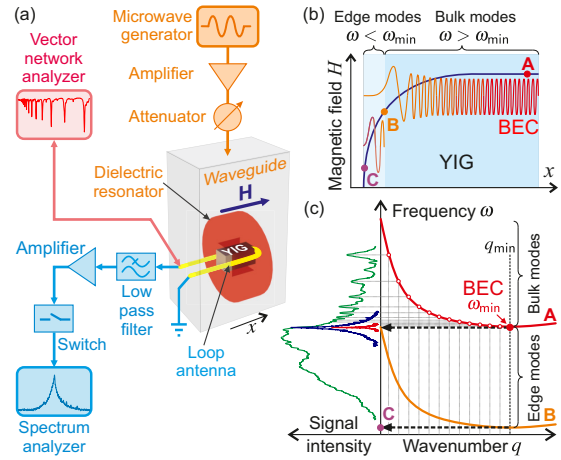

FIG. 1. (a) The experimental setup for microwave detection of magnon dynamics. Different parts of the setup are color coded: Orange denotes the pumping circuit, blue highlights the receiving circuit, and red marks the test circuit. (b) Schematic representation of the bulk BEC mode and one of the edge magnon modes in a cuboid YIG sample. The monotonic blue line shows the profile of the static magnetic field **H** within the YIG sample. Color points denote three field values: A, deeply inside the sample; B, at the point near the sample edge, where the bulk BEC mode becomes evanescent with purely imaginary wave number; and C, at the sample edge. (c) Schematic representation of magnon dispersion curves in the middle of the sample (at point A) and near the edge (at point B). The green, blue, and red signal intensity lines represent the microwave power spectra from the YIG sample registered during 1 μs interval before the end of pumping, and 2 and 4 μs after the pump pulse is turned off, respectively.

$\omega[q(x), H(x)] = \omega_{\min} = \omega(q_{\min}, H_{\rm A})$, providing a relation between $q(x)$ and $H(x)$.

The bulk frequency spectrum $\omega(q, H_{\rm A})$ is schematically shown by the red line in the upper part of Fig. 1(c). As one moves from point A to some point B near the sample edge, the magnetic field decreases and the spectrum branch $\omega[q(x), H(x)]$ is continuously shifted down. The spectrum $\omega(q, H_{\rm B})$ for the lower magnetic field at point B is schematically shown by the orange line in the lower part of Fig. 1(c). Therefore, according to the equation for $\omega_{\min}$, the wave number $q(x)$ of the BEC magnons with $\omega[q(x), H(x)] = \omega_{\min}$ decreases towards the edges of the sample, reaching zero value for $x = x_{\rm B}$ as is indicated by the black dashed arrow in Fig. 1(c). For $x < x_{\rm B}$, the bulk mode becomes evanescent with a purely imaginary wave number. In the near-edge region, between points B and C, only localized edge modes exist. A small value of $q(x)$ near point B, and, correspondingly, a large wavelength of magnons, enhances the coupling of the magnon BEC with the electromagnetic field.

The large volume of the sample and its cuboidal shape make it possible to achieve the desired detection sensitivity using a simple inductive loop antenna placed around the sample and connecting to the receiving circuit marked in blue in Fig. 1(a). The fast microwave switch is used to measure power-frequency radiation spectra $J_{\rm rad}(\omega, t)$ in 1-μs-long time windows shifted by 0.5 μs steps. The low-pass filter protects the spectrum analyzer from a strong

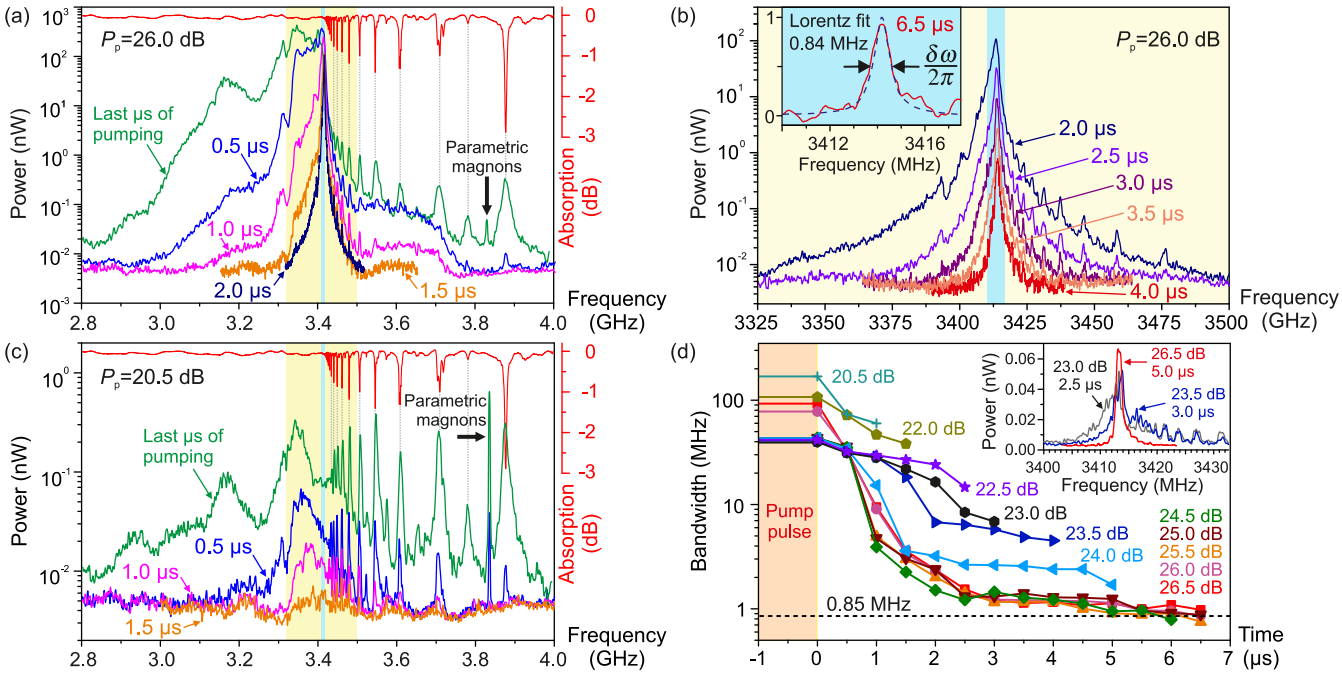

FIG. 2. Magnon radiation spectra $J_{\rm rad}(\omega, t)$ for two pumping powers $P_{\rm p}$ and $\mu_0 H = 115$ mT. (a)–(c) The spectra are taken at consequent moments of time before [green line in (a) and (c)] and after switching off the pumping power. The yellow and blue shading in (a)–(c) denotes the frequency range: Yellow shading in (a) corresponds to the spectra shown in (b), and blue shading corresponds to the spectrum shown in the inset in (b). The absorption spectrum $J_{\rm abs}(\omega, t)$ measured without pumping is shown in (a) and (c) by the red lines. The linewidth of bulk modes near the bottom of the spectrum is slightly below 1 MHz. The inset in (c) shows the BEC's spectral line normalized by its maximum value. A Lorentz fit is shown by the black dashed line. (d) Time evolution of the signal bandwidth for different pumping powers $P_{\rm p}$. The black dashed line in (d) marks the mean value of the linewidth $\delta\omega_{\rm fin}/(2\pi) \approx 0.85$ MHz in the later stage of the BEC evolution. The inset demonstrates the narrowing of the radiation spectrum of the freely evolving magnon gas with an increase of the pumping power $P_{\rm p}$. The different delay times are chosen to have approximately the same maximum magnitude for the three spectra shown.

pumping signal. Magnons are pumped by 6-μs-long pulses of the electromagnetic field of frequency $\omega_{\rm p} = 2\pi \cdot 7.68$ GHz, whose amplitude is enhanced by a dielectric resonator [see Fig. 1(a), where the orange circuitry illustrates the pumping circuit].

Consider first the structure of the eigenmodes of the cuboid sample. Their absorption spectrum $J_{\rm abs}(\omega, t)$, measured by a vector network analyzer and colored in red in Fig. 1(a), is shown by the red line in Fig. 2(a). In the same figure, the green line denotes the radiation spectrum $J_{\rm rad}(\omega, t)$ of the sample measured during the last microsecond of pumping. Above $\omega/(2\pi) > 3.414$ GHz, one can see a set of discrete peaks, whose frequencies coincide [49] in both spectra [see the thin vertical dashed lines in Fig. 1(a)]. They originate from the bulk magnon modes, schematically shown on the magnon dispersion branch A in Fig. 1(c). In an infinite sample, the spectrum of such modes is continuous. However, in the finite sample, only a discrete set of wave numbers q_n is allowed. In the simple case of a longitudinally magnetized bar of length L, the periodic boundary conditions dictate $q_n = 2\pi n/L$. They are illustrated in Fig. 1(c) by gray dotted vertical lines. The corresponding "allowed" values of $\omega = \omega_n = \omega(q_n)$ are shown by open dots and horizontal gray lines. Larger values of $\omega(q_n)$ correspond to smaller q_n, which are better coupled with the inductive loop. This explains why the peaks at higher frequencies are more pronounced in Fig. 2(a). Furthermore, the peak positions become closer as ω approaches $\omega_{\rm min}$ from above. This behavior is well reproduced by the spectra in Fig. 2(a), where $\omega_{\rm min}/(2\pi) = 3.414$ GHz.

The part of the spectra at $\omega < \omega_{\rm min}$ originates from the modes localized near the sample edges. Indeed, the decreasing intrinsic magnetic field [blue line in Fig. 1(b)] between B and the edge of the sample serves as a potential well. In this well, there exists a discrete set of magnon states having a relatively large characteristic scale. These edge modes are well coupled with the electromagnetic field around the sample and therefore are affected by additional radiation damping. Since the additional damping results in a low quality factor of these modes, their discrete structure is hardly visible in the radiation spectrum. For the same reason, these modes practically do not contribute to the absorption spectrum. Note also that the actual positions of the peaks in Fig. 2(a) are not so regular as expected from the one-dimensional model. In a finite sample of a general shape, the role of "allowed" ω_n is played by the frequencies of so-called Walker modes in a cuboid, which may be not equidistant [50,51].

Consider now the evolution of the radiation spectrum $J_{\rm rad}(\omega, t)$ at a sufficiently strong pump power $P_{\rm p} = 26.0$ dB above the threshold of the parametric instability. During the pumping, it extends from 2.8 to 4 GHz as is indicated by the green line in Fig. 2(a). The main radiation power is located in the 80 MHz band around $\omega_{\rm min}$. Such a large width is caused by intensive shaking of the entire magnon frequency spectra by a powerful microwave pumping field. For instance, for

$P_p = 26.0$ dB, the amplitude of the microwave pumping field h_p applied parallel to the bias magnetic field H is estimated to be about 23 Oe. As a result, the magnon frequency spectrum moves up and down in the range of ± 65 MHz, which is close to the radiation spectrum width.

After switching off the pumping power, the shaking of the magnon frequencies ceases and the spectrum width quickly decreases as seen in Figs. 2(a) and 2(b). The edge modes with $\omega < \omega_{min}$ uniformly decay within the first 2 μs, likely due to effective radiation damping. The evolution of the bulk modes with $\omega \gtrsim \omega_{min}$ is more complicated. The most intense peaks in the initial spectrum are strongly decreased already within a time interval of 0.5 μs, especially at frequencies, for which the radiation damping is most efficient. Another reason for the spectrum narrowing is the redistribution of magnons towards modes with $\omega \simeq \omega_{min}$ during the BEC formation.

In Fig. 2(b), we show details of the further evolution of $J_{rad}(\omega, t)$. Here, we plot the spectra for more narrow frequency intervals, colored in Fig. 2(a) by yellow and blue shading, respectively. The width of the spectra measured with time delays $t_d = (2–4)$ μs decreases further [see Fig. 2(b)], confirming the process of gathering the magnons toward the BEC state at $\omega = \omega_{min}$. Over time, the spectra evolve into a single spectral line of Lorentzian shape, as shown in the inset in Fig. 2(b).

The situation develops differently at lower pumping powers [see Fig. 2(c) for $P_p = 20.5$ dB]. The shown spectra have the same structure of the bulk and edge modes as in Fig. 2(a). However, no BEC formation occurs at the bottom of the bulk modes' frequency spectrum within the interval indicated by the blue shading.

To quantify the radiation spectra, we investigate their bandwidth $\delta\omega$ [52]. Its evolution for different P_p from 20.5 to 26.5 dB is shown in Fig. 2(d). After the pumping is turned off, $\delta\omega$ decreases monotonically due to the Bose-Einstein condensation process. This process is dominated by four-magnon scattering processes with a rate proportional to N^2 [25,27], where N is the number of bottom magnons. Increasing N at larger P_p leads to more efficient magnon gathering toward ω_{min} and a faster decrease in $\delta\omega$. This narrowing has a threshold character and occurs when the pumping power increases from 22.5 to 24 dB. We consider this as evidence of magnon condensate formation at $P_p \gtrsim 24$ dB.

The inset in Fig. 2(d) presents $J_{rad}(\omega, t)$ spectra measured near the detection limit of the experimental setup for two low pumping powers of $P_p = 23.0$ and 23.5 dB, and for the highest value of $P_p = 26.5$ dB. Being rather weak, they correspond to the final stages of the evolution of the magnon system at the bottom of their spectrum, when no nonlinear scattering is expected and both condensed and gaseous magnons linearly decay to the thermal phonon bath. However, the structure of these residual spectra is determined by the previous processes of nonlinear four-magnon scattering and BEC formation. For weaker pumping, the spectral line at ω_{min} is surrounded by a distribution of relatively strongly populated magnon modes, which demonstrate a clear comblike structure at frequencies above ω_{min}. Increasing pumping power leads to the depopulation of all these modes due to magnon gathering toward the dense BEC. As a result, only the spectral line related to the magnon condensate remains in the spectrum. A similar long-living BEC on the ground energy level was reported in ^{3}He [42] and understood as a magnon time crystal [45].

Probably the most important evidence for full coherency, as shown in Fig. 2, is that at later times (say, for $t_d > 2.5$ μs) the exponentially decaying residual spectra for $P_p \geqslant 24$ dB have a Lorentzian shape with the bandwidth $\delta\omega$ approaching the value of about $\delta\omega_{fin}/(2\pi) \simeq 0.85$ MHz, almost independent of P_p.

Concluding the discussion of Fig. 2(d), we note that one has to distinguish between (i) the moment when the coherent component appears in the magnon gas and (ii) the state in which most of the magnons near the bottom of the spin-wave spectrum are already condensed. We interpret the sharp narrowing of the magnon spectrum immediately after the pumping termination [see, e.g., the red line corresponding to 26.5 dB in Fig. 2(d)] as evidence that the first stage occurs in a time interval noticeably shorter than 1 μs. The second stage is reached in the time interval from 1.0 to 2.5 μs, as seen from the BEC linewidth's approximate saturation for times t_d after this characteristic time interval. The further narrowing is caused by a decrease in the gaseous magnons' density in the BEC vicinity, which leads to a smaller disturbance in the lowest energy level bandwidth.

Thus, the magnon system evolving toward BEC reaches full coherence, with the width of the magnon radiation spectrum decreasing by more than two orders of magnitude. The residual bandwidth is mainly determined by the lifetime of magnons, as expected for a fully coherent BEC consisting of a single magnon state. We believe that this thorough analysis of the temporal evolution of the overpopulated magnon gas toward a fully coherent magnon BEC in its unperturbed state represents an important step forward in understanding the behavior of the magnon condensate. Moreover, our results show that further increasing the applied power does not lead to a loss of coherence of the BEC state, demonstrating the stability of this state at higher pumping levels. This allows high densities of this coherent state, resulting in easily detectable high amplitude signals, bringing the realization of room-temperature BEC-based computations closer.

Moreover, we show that the magnon BEC coupling with dynamic stray fields outside the sample is enabled by a proper choice of the sample shape giving direct spectroscopic access to the BEC. Such an approach can function as a convenient tool for integrating magnetic quantum systems into electrical environments. It opens a way to control the magnon condensate's characteristics by the resonant excitation of neighboring magnon modes, particularly to obtain a long-lived condensate after the pumping pulse. This control should also help to better elucidate the fundamental problem of the smooth fusion of classical physics with quantum mechanics by investigating the limitations and decay of quantum coherence in mesoscopic condensed systems.

This research was funded by the European Research Council within the Advanced Grant No. 694709 SuperMagnonics and by the Deutsche Forschungsgemeinschaft (DFG, German Research Foundation) within the Transregional Collaborative Research Center–TRR 173–268565370 "Spin+X" (projects B01, B04). The authors are grateful to G. A. Melkov and H. Yu. Musiienko-Shmarova for fruitful discussions.

[1] A. D. Stone, *Einstein and the Quantum: The Quest of the Valiant Swabian* (Princeton University Press, Princeton, NJ, 2015).

[2] A. Einstein, Quantentheorie des einatomigen idealen Gases, Sitzungsber. Preuss. Akad. Wiss., Phys.-Math. Kl. **22**, 261 (1924).

[3] V. Bose, Plancks Gesetz und Lichtquantenhypothese, Z. Phys. **26**, 178 (1924).

[4] H. Fröhlich, Bose condensation of strongly excited longitudinal electric modes, Phys. Lett. A **26**, 402 (1968).

[5] D. Snoke, Coherent questions, Nature (London) **443**, 403 (2006).

[6] K. B. Davis, M.-O. Mewes, M. R. Andrews, N. J. van Druten, D. S. Durfee, D. M. Kurn, and W. Ketterle, Bose-Einstein Condensation in a Gas of Sodium Atoms, Phys. Rev. Lett. **75**, 3969 (1995).

[7] M. H. Anderson, J. R. Ensher, M. R. Matthews, C. E. Wieman, and E. A. Cirnell, Observation of Bose-Einstein condensation in a dilute atomic vapor, Science **269**, 198 (1995).

[8] A. Amo, J. Lefrère, S. Pigeon, C. Adrados, C. Ciuti, I. Carusotto, R. Houdré, E. Giacobino, and A. Bramati, Superfluidity of polaritons in semiconductor microcavities, Nat. Phys. **5**, 805 (2009).

[9] J. P. Eisenstein and A. H. MacDonald, Bose-Einstein condensation of excitons in bilayer electron systems, Nature (London) **432**, 691 (2004).

[10] J. Klaers, J. Schmitt, F. Vewinger, and M. Weitz, Bose-Einstein condensation of photons in an optical microcavity, Nature (London) **468**, 545 (2010).

[11] Yu. M. Bunkov and G. E. Volovik, Bose-Einstein condensation of magnons in superfluid ^{3}He, J. Low Temp. Phys. **150**, 135 (2008).

[12] S. O. Demokritov, V. E. Demidov, O. Dzyapko, G. A. Melkov, A. A. Serga, B. Hillebrands, and A. N. Slavin, Bose-Einstein condensation of quasi-equilibrium magnons at room temperature under pumping, Nature (London) **443**, 430 (2006).

[13] A. A. Serga, V. S. Tiberkevich, C. W. Sandweg, V. I. Vasyuchka, D. A. Bozhko, A. V. Chumak, T. Neumann, B. Obry, G. A. Melkov, A. N. Slavin, and B. Hillebrands, Bose-Einstein condensation in an ultra-hot gas of pumped magnons, Nat. Commun. **5**, 3452 (2014).

[14] M. Schneider, T. Brächer, D. Breitbach, V. Lauer, P. Pirro, D. A. Bozhko, H. Yu. Musiienko-Shmarova, B. Heinz, Q. Wang, T. Meyer, F. Heussner, S. Keller, E. Th. Papaioannou, B. Lägel, T. Löber, C. Dubs, A. N. Slavin, V. S. Tiberkevich, A. A. Serga, B. Hillebrands, and A. V. Chumak, Bose-Einstein condensation of quasiparticles by rapid cooling, Nat. Nanotechnol. **15**, 457 (2020).

[15] K. Nakata, K. A. van Hoogdalem, P. Simon, and D. Loss, Josephson and persistent spin currents in Bose-Einstein condensates of magnons, Phys. Rev. B **90**, 144419 (2014).

[16] Y. Tserkovnyak and M. Kläui, Exploiting Coherence in Nonlinear Spin-Superfluid Transport, Phys. Rev. Lett. **119**, 187705 (2017).

[17] T. Byrnes and Y. Yamamoto, Macroscopic quantum computation using Bose-Einstein condensates, Phys. Rev. A **85**, 040306(R) (2012).

[18] S. N. Adrianov and S. A. Moiseev, Magnon qubit and quantum computing on magnon Bose-Einstein condensates, Phys. Rev. A **90**, 042303 (2014).

[19] Y. Xue, I. Chestnov, E. Sedov, E. Kiktenko, A. K. Fedorov, S. Schumacher, X. Ma, and A. Kavokin, Split-ring polariton condensates as macroscopic two-level quantum systems, Phys. Rev. Research **3**, 013099 (2021).

[20] S. Ghosh and T. C. H. Liew, Quantum computing with exciton-polariton condensates, npj Quantum Inf. **6**, 16 (2020).

[21] F. Arute, K. Arya, R. Babbush, D. Bacon, J. C. Bardin, R. Barends, R. Biswas, S. Boixo, F. G. S. L. Brandao, D. A. Buell, B. Burkett, Y. Chen, Z. Chen, B. Chiaro, R. Collins, W. Courtney, A. Dunsworth, E. Farhi, B. Foxen, A. Fowler *et al.*, Quantum supremacy using a programmable superconducting processor, Nature (London) **574**, 505 (2019).

[22] V. Cherepanov, I. Kolokolov, and V. S. L'vov, The saga of YIG: spectra, thermodynamics, interaction and relaxation of magnons in a complex magnet, Phys. Rep. **229**, 81 (1993).

[23] D. A. Bozhko, A. A. Serga, P. Clausen, V. I. Vasyuchka, F. Heussner, G. A. Melkov, A. Pomyalov, V. S. L'vov, and B. Hillebrands, Supercurrent in a room-temperature Bose-Einstein magnon condensate, Nat. Phys. **12**, 1057 (2016).

[24] E. Schlömann, Longitudinal susceptibility of ferromagnets in strong rf fields, J. Appl. Phys. **33**, 527 (1962).

[25] V. S. L'vov, *Wave Turbulence Under Parametric Excitation: Applications to Magnets* (Springer, Berlin, 1994).

[26] V. E. Demidov, O. Dzyapko, S. O. Demokritov, G. A. Melkov, and A. N. Slavin, Thermalization of a Parametrically Driven Magnon Gas Leading to Bose-Einstein Condensation, Phys. Rev. Lett. **99**, 037205 (2007).

[27] V. E. Zakharov, V. S. L'vov, and G. Falkovich, *Kolmogorov Spectra of Turbulence I: Wave Turbulence* (Springer, Berlin, 1992).

[28] V. E. Demidov, O. Dzyapko, S. O. Demokritov, G. A. Melkov, and A. N. Slavin, Observation of Spontaneous Coherence in Bose-Einstein Condensate of Magnons, Phys. Rev. Lett. **100**, 047205 (2008).

[29] A. J. E. Kreil, H. Y. Musiienko-Shmarova, S. Eggert, A. A. Serga, B. Hillebrands, D. A. Bozhko, A. Pomyalov, and V. S. L'vov, Tunable space-time crystal in room-temperature magnetodielectrics, Phys. Rev. B **100**, 020406(R) (2019).

[30] P. Nowik-Boltyk, O. Dzyapko, V. E. Demidov, N. G. Berloff, and S. O. Demokritov, Spatially non-uniform ground state and quantized vortices in a two-component Bose-Einstein condensate of magnons, Sci. Rep. **2**, 482 (2012).

[31] D. A. Bozhko, A. J. E. Kreil, H. Yu. Musiienko-Shmarova, A. A. Serga, A. Pomyalov, V. S. L'vov, and B. Hillebrands, Bogoliubov waves and distant transport of magnon condensate at room temperature, Nat. Commun. **10**, 2460 (2019).

[32] A. J. E. Kreil, A. Pomyalov, V. S. L'vov, H. Yu. Musiienko-Shmarova, G. A. Melkov, A. A. Serga, and B. Hillebrands, Josephson oscillations in a room-temperature Bose-Einstein magnon condensate, arXiv:1911.07802.

[33] A. J. E. Kreil, D. A. Bozhko, H. Yu. Musiienko-Shmarova, V. I. Vasyuchka, V. S. L'vov, A. Pomyalov, B. Hillebrands, and A. A. Serga, From Kinetic Instability to Bose-Einstein Condensation and Magnon Supercurrents, Phys. Rev. Lett. **121**, 077203 (2018).

[34] L. Mihalceanu, D. A. Bozhko, V. I. Vasyuchka, A. A. Serga, B. Hillebrands, A. Pomyalov, V. S. L'vov, and V. S. Tiberkevich, Magnon Bose-Einstein condensate and supercurrents over a wide temperature range, Ukr. J. Phys. **64**, 927 (2019).

[35] O. Dzyapko, P. Nowik-Boltyk, B. Koene, V. E. Demidov, J. Jersch, A. Kirilyuk, T. Rasing, and S. O. Demokritov, High-resolution magneto-optical Kerr-effect spectroscopy of magnon Bose-Einstein condensate, IEEE Magn. Lett. **7**, 3501805 (2016).

[36] O. Dzyapko, I. Lisenkov, P. Nowik-Boltyk, V. E. Demidov, S. O. Demokritov, B. Koene, A. Kirilyuk, T. Rasing, V. Tiberkevich, and A. Slavin, Magnon-magnon interactions in a room-temperature magnonic Bose-Einstein condensate, Phys. Rev. B **96**, 064438 (2017).

[37] O. Dzyapko, V. E. Demidov, S. O. Demokritov, G. A. Melkov, and V. L. Safonov, Monochromatic microwave radiation from the system of strongly excited magnons, Appl. Phys. Lett. **92**, 162510 (2008).

[38] S. M. Rezende, Theory of coherence in Bose-Einstein condensation phenomena in a microwave-driven interacting magnon gas, Phys. Rev. B **79**, 174411 (2009).

[39] A. S. Borovik-Romanov, Yu. M. Bunkov, V. V. Dmitriev, V. Makroczyova, Yu. M. Mukharskii, D. A. Sergatskov, and A. de Waard, The analog of the Josephson effect in the spin supercurrent, J. Phys. Colloques **49**, C8-2067 (1988).

[40] D. J. Cousins, S. N. Fisher, A. I. Gregory, G. R. Pickett, and N. S. Shaw, Persistent Coherent Spin Precession in Superfluid ^{3}He-*B* Driven by Off-Resonant Excitation, Phys. Rev. Lett. **82**, 4484 (1999).

[41] V. B. Eltsov, R. De Graaf, M. Krusius, and D. E. Zmeev, Vortex core contribution to textural energy in ^{3}He-B below $0.4T_c$, J. Low Temp. Phys. **162**, 212 (2011).

[42] S. Autti, Y. M. Bunkov, V. B. Eltsov, P. J. Heikkinen, J. J. Hosio, P. Hunger, M. Krusius, and G. E. Volovik, Self-Trapping of Magnon Bose-Einstein Condensates in the Ground State and on Excited Levels: From Harmonic to Box Confinement, Phys. Rev. Lett. **108**, 145303 (2012).

[43] P. J. Heikkinen, S. Autti, V. B. Eltsov, J. J. Hosio, M. Krusius, and V. V. Zavjalov, Relaxation of Bose-Einstein condensates of magnons in magneto-textural traps in superfluid ^{3}He-B, J. Low Temp. Phys. **175**, 3 (2014).

[44] S. Autti, V. V. Dmitriev, J. T. Mäkinen, J. Rysti, A. A. Soldatov, G. E. Volovik, A. N. Yudin, and V. B. Eltsov, Bose-Einstein Condensation of Magnons and Spin Superfluidity in the Polar Phase of ^{3}He, Phys. Rev. Lett. **121**, 025303 (2018).

[45] S. Autti, V. B. Eltsov, and G. E. Volovik, Observation of a Time Quasicrystal and its Transition to a Superfluid Time Crystal, Phys. Rev. Lett. **120**, 215301 (2018).

[46] Y. M. Bunkov, P. M. Vetoshko, A. N. Kuzmichev, G. V. Mamin, S. B. Orlinskii, T. R. Safin, V. I. Belotelov, and M. S. Tagirov, Long-lived induction signal in yttrium iron garnet, JETP Lett. **111**, 62 (2020).

[47] E. Schlömann, Generation of spin waves in nonuniform magnetic fields. I. Conversion of electromagnetic power into spin-wave power and vice versa, J. Appl. Phys. **35**, 159 (1964).

[48] K. R. Smith, M. J. Kabatek, P. Krivosik, and M. Wu, Spin wave propagation in spatially nonuniform magnetic fields, J. Appl. Phys. **104**, 043911 (2008).

[49] In fact, the frequencies of the peaks of the radiation spectrum measured during pump action are 14 MHz higher than the frequencies of the corresponding peaks in all other radiation and absorption spectra. This difference arises due to decrease in the sample magnetization caused by pumping magnons. To demonstrate the identity of the structure of all spectra, we shifted this radiation spectrum [the green line in Fig. 2(a)] down by 14 MHz.

[50] A. G. Gurevich and G. A. Melkov, *Magnetization Oscillations and Waves* (CRC Press, Boca Raton, FL, 1996).

[51] M. Elyasi, Y. M. Blanter, and G. E. W. Bauer, Resources of nonlinear cavity magnonics for quantum information, Phys. Rev. B **101**, 054402 (2020).

[52] For single-peak spectra, we chose $\delta\omega$ as the peak width at the half-maximum magnitude. This definition corresponds to the width of the Lorentz peak, describing a uniformly broadened spectral line. For the spectra with complex many-peak structures, such as the spectra in Fig. 2, we generalize this definition as follows, $\delta\omega = [2\int \Omega^2 \widetilde{f}(\Omega)d\Omega / \int \widetilde{f}(\Omega)d\Omega]^{1/2}$, where $\Omega = \omega - \omega_{\min}$ and $\widetilde{f}(\Omega)$ is the truncated spectrum $f(\Omega)$, with the spectrum part below 5.5% of its maximum magnitude removed.